THE JOURNAL OF PHYSICAL CHEMISTRY B

pubs.acs.org/JPCB Article

Biological Nanopore Probe: Probing of Viscous Solutions in a Confined Nanospace

Masaki Matsushita, Kan Shoji, Natsumi Takai, and Ryuji Kawano*

Cite This: J. Phys. Chem. B 2020, 124, 2410–2416 Read Online

ACCESS | Metrics & More | Article Recommendations | Supporting Information

ABSTRACT: This paper describes a nanospace probing system constructed with a pore-forming toxin and a hairpin DNA (hpDNA) molecule. The single hpDNA molecule can be inserted and can move in the confined nanospace of the alpha-hemolysin (αHL) pore. The molecular motion of the hpDNA can be determined based on the fluctuation of the blocking current via channel current measurements. Using this system, we investigated the effect of viscosity of the aqueous solution in the macrospace (bulk) and in the confined nanospace with a small molecule (glycerol) and a polymer (PEG600). The molecular motion of the hpDNA in the nanospace differed in glycerol and PEG600 solutions, while the viscosity remained the same in the bulk solution. The fundamental factors for the viscosity in glycerol and PEG600 solutions are hydrogen bonding and the entanglement of polymer chains, respectively. This difference in factors becomes significant in confined nanospaces, and our system allows us to observe its effect. Additionally, we constructed a spatially resolved nanopore probe integrated into a gold nanoneedle. The αHL–hpDNA nanoprobe system was constructed with the nanoneedle and can be used to monitor the nanospace with nanometer spatial resolution.

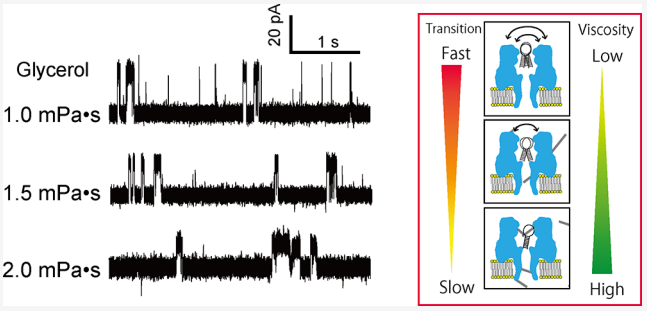

INTRODUCTION

The physicochemical properties of aqueous solutions are strongly influenced by temperature and pressure. Specifically, these solutions have freezing and boiling points that depend on the ambient temperature and pressure. It is also known that the size of the space they occupy significantly affects their physicochemical properties, referred to as confinement effects.[1−7] For instance, the phase transition of aqueous solutions in nanospace exhibits unusual behavior owing to confinement effects; water freezes and generates cubic ice at −13 °C in 9 nm diameter silicate pores.[4] The mechanism for this behavior is explained by the theory on depression of the freezing point of water below a critical confinement length scale (ca. 2.5 nm), described by continuum thermodynamics and the Gibbs–Thomson effect.[2,8,9] In contrast, the freezing temperature of water inside an isolated carbon nanotube with a diameter of approximately 1 nm is much higher than the theoretical prediction.[8]

The confinement effect can be investigated experimentally from either of two viewpoints: one focuses on the kinds of materials that can be used to construct the confined nanospace, and the other focuses on estimation of the physicochemical properties of solutions in the confined space. With respect to the type of materials, porous silica samples (Spherisorb or Gasil) have been used as nanospace confining materials in early studies.[1−4] Subsequently, various materials, such as sol–gel glasses, silica gels, zeolites, polymers, carbon, metal–organic framework, and reversed micelles, have been used to make the confined nanospace.[1] In addition, nanofluidic technology has been used for extended nanospaces.[10,11] The size of the confined space of porous materials ranges from 1 nm to several microns. Using these materials, physicochemical properties such as supercooling or nucleation behavior have been estimated and the anomalous properties due to confinement studied using methods such as NMR,[10,12] neutron scattering,[1,3,5,7] thermal calorimetry,[13,14] and molecular dynamic simulations.[15,16] Spectroscopy can reveal the behavior of the molecule inside the confined space but requires highly transparent materials. In addition, the low sensitivity of spectrometry to water molecules is an issue. Further, the data obtained from conventional porous materials are the ensemble average and have a wide distribution owing to the size distribution of the nanospace. Recently, isolated carbon nanotubes have been used as a confining material with known size.[6,8,17] The phase transition of water in nanotubes observed by Raman spectroscopy was found to be sensitive to the carbon nanotube diameter, and the results revealed large temperature variations of freezing transition (by as much as 100 °C) in this system.[8] Although isolated and single

Received: November 27, 2019
Revised: February 5, 2020
Published: February 7, 2020

Downloaded via KYOTO UNIV on July 31, 2020 at 08:15:38 (UTC).
See https://pubs.acs.org/sharingguidelines for options on how to legitimately share published articles.

ACS Publications © 2020 American Chemical Society

https://dx.doi.org/10.1021/acs.jpcb.9b11096
J. Phys. Chem. B 2020, 124, 2410–2416

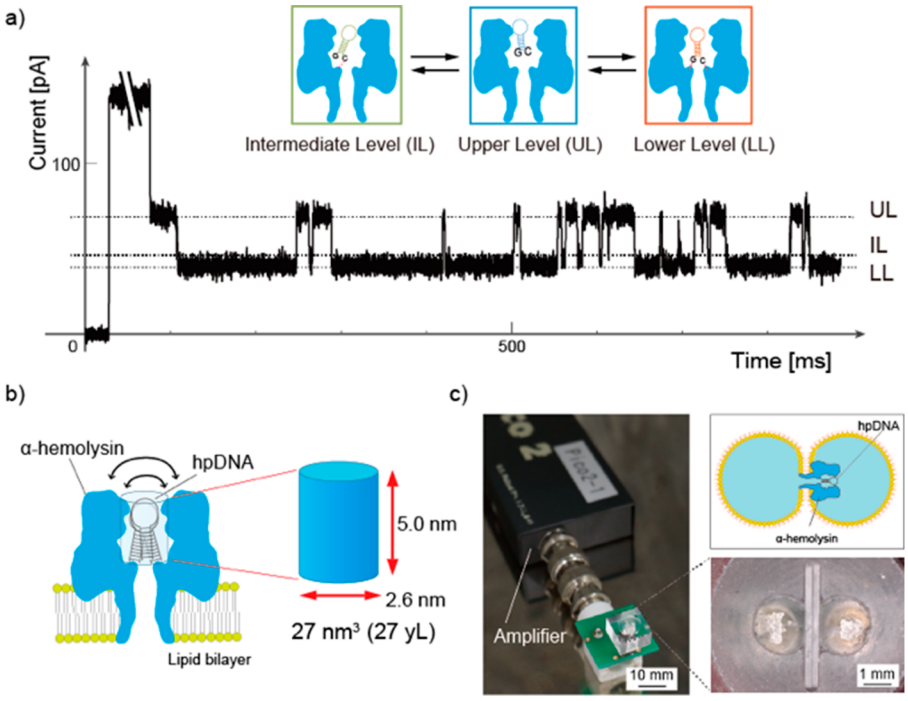

Figure 1. Illustration of the nanopore probe. (a) A typical current through the nanopore probe and schematic illustration of the αHL nanopore and hpDNA states. (b) Lipid bilayers are prepared by the droplet contact method. αHL is reconstituted in the lipid bilayer, and hpDNA is inserted into the pore. (c) Photograph of the device for measuring channel currents.

nanospaces have an essential role in studying confinement effects, the development of confining materials and probing methods is still challenging.

Here, we report on a single confined space using a biological nanopore, alpha-hemolysin (αHL) (Figure 1). αHL is a pore-forming toxin produced by *Staphylococcus aureus* and forms a mushroom-like nanopore structure in the lipid bilayer with a cylindrical vestibule of 5 nm height and 2.6 nm diameter (volume is ca. 27 nm^3 = 27 yoctoL) inside the nanopore (Figure 1b).[18,19] This nanopore protein has been used for DNA sequencing[20−23] and single molecule detection[19,24−33] by measuring the ionic current through the nanopore. A single-stranded DNA (ssDNA) can pass through this nanopore, whereas double-stranded DNA (dsDNA) cannot because the diameter of the restricted region of the nanopore is 1.4 nm.[19] Using this unique geometrical feature, Vercoutere et al. studied the orientation of hairpin DNA (hpDNA) with nine base pairs in the nanopore at the single molecule level.[34−36] They reported that hpDNA is trapped in the vestibule and mainly shows three distinctive current signals, upper level (**UL**), intermediate level (**IL**), and lower level (**LL**), as shown in Figure 1a. These three current levels reflect the three different orientations of hpDNA in the vestibule.[36] Based on this information, we propose that the movement of hpDNA in the nanopore could also signal the solution properties in the confined space; for instance, the solution viscosity in the confined space can be investigated by analyzing the blocking current signals. In this study, we used two different viscous solutions with a similar viscosity range (specifically, glycerol and PEG600) and analyzed the movement of hpDNA in order to understand the effect of viscosity in the confined nanospace. Based on our results, nanopore probes comprised of nanopores with hpDNA will be a useful tool for observing the physical chemistry of confined nanospaces.

METHODS

Reagents and Chemicals. All aqueous solutions were prepared with ultrapure water from a Milli-Q system (Millipore, Billerica, MA, USA). The reagents were as follows: 1,2-diphytanoyl-*sn*-glycero-3-phosphocholine (DPhPC; Avanti Polar Lipids, Alabaster, AL, USA), *n*-decane (Wako Pure Chemical Industries, Ltd., Osaka, Japan), glycerol (Wako Pure Chemical Industries, Ltd., Osaka, Japan), polyethylene glycol 600 (PEG600; Tokyo Chemical Industry Co., Ltd., Tokyo, Japan), potassium chloride (KCl; Nacalai Tesque), potassium nitrate (KNO_3; Sigma-Aldrich), calcium chlorite ($CaCl_2$; Sigma-Aldrich, St. Louis, MO, USA), and *O*-(3-carboxypropyl)-*O*′-[2-(3-mercaptopropionylamino) ethyl]propylethylene glycol with molecular weight 3000 (thiol-PEG; Sigma-Aldrich, St. Louis, MO, USA).

Buffered electrolyte solutions were prepared from ultrapure water, which was obtained from a Milli-Q system (Millipore, Billerica, MA, USA). αHL (Sigma-Aldrich, St. Louis, MO, USA), obtained as a monomer protein isolated from *Staphylococcus aureus* in the form of a powder, was rehydrated at a concentration of 1 mg/mL in ultrapure water and stored at −80 °C. For use, samples were diluted to 0.5 μM using a buffered electrolyte solution and stored at 4 °C. Hairpin DNA (GTTCGAACGTTTTCGTTCGAAC) synthesized by FASMAC Co., Ltd., Kanagawa, Japan, in the form of a powder, was dissolved at a concentration of 100 μM in ultrapure water and stored at −20 °C as the stock solution.

Lipid Bilayer Preparation and Reconstitution Hemolysin. Bilayer lipid membranes (BLMs) were prepared using a microfabricated device (Figure 1c), as previously reported.[37,38] BLMs can be simultaneously formed in this device by the droplet contact method. First, the DPhPC (lipids/*n*-decane, 10 mg/mL) solution (2.3 μL) was poured into each chamber. Next, the buffer solution (4.7 μL) without αHL and hpDNA was poured

https://dx.doi.org/10.1021/acs.jpcb.9b11096
J. Phys. Chem. B 2020, 124, 2410−2416

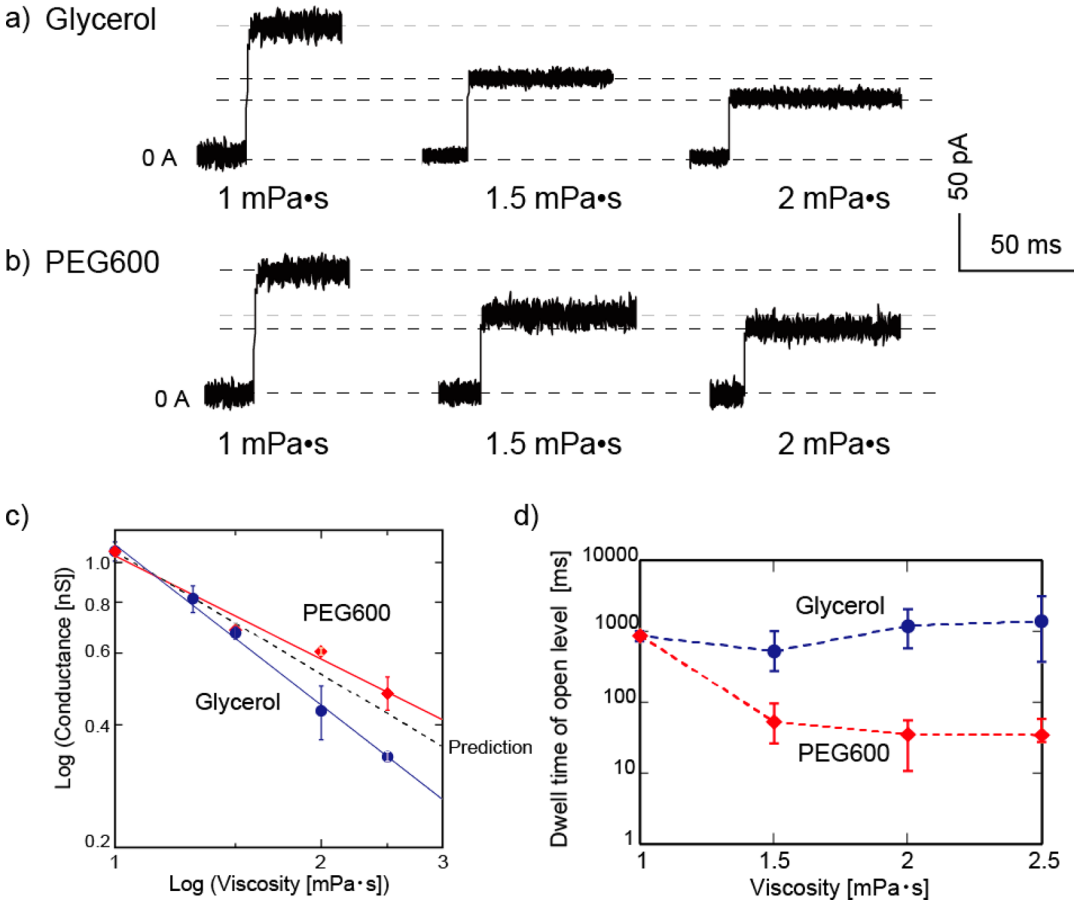

Figure 2. Result of nanopore probe measurement of pore conductance. (a, b) Typical current and time traces in the presence of (a) glycerol and (b) PEG600 (V_{app} = +120 mV). (c) The conductance in each viscosity of glycerol (blue line) and PEG600 (red line). The black-dashed line is prediction from bulk viscosity. (d) Dwell time of each solution. The dwell time is from pore opening to hpDNA insertion.

into each recording chamber. The buffer solution (4.7 μL) with αHL (final concentration: 0.01 μM) and hpDNA (final concentration: 5 μM) was poured into each ground chamber. In this study, the buffer solution (1 M KCl, 10 mM MOPS, pH 7.0) was used for all droplets. A few minutes after adding the buffer solution, the two lipid monolayers connected and formed BLMs, and αHL formed nanopores by reconstitution in the BLMs. When the BLMs ruptured, they were reformed by tracing with a hydrophobic stick between two droplets.

Channel Current Measurements and Data Analysis. Channel current was monitored using a Pico patch-clamp amplifier (Tecella, Foothill Rantch, CA) connected to each chamber. Ag/AgCl electrodes were already present in each droplet when the solution was added to the chambers. A constant voltage of +120 mV for most of the experiments or +100 mV for the nanoneedle experiments was applied to the recording chamber, and the other chamber was connected to ground. The solution conductivity and viscosity were used from an electrochemical handbook and the previous reports,[39,40] respectively. Reconstituted αHL in BLMs allowed ions to pass through a nanopore under the voltage gradient, and channel current signals were obtained. When hpDNA was present in the ground chamber, the αHL nanopore was blocked by the captured hpDNA, and the channel current decreased to approximately half that of the open state and exhibited three individual current states. The **UL**, **IL**, and **LL** states were determined by selecting the peak top using Origin software. When **IL** and **LL** states were unseparated in the blocking current analysis, we determined each state using the duration time (Figure S2). We subsequently analyzed the blocking amplitude and the duration time of the three states. The signals were detected using an 8 kHz low-pass filter at a sampling frequency of 40 kHz. Analysis of channel current signals and duration time was performed using pCLAMP ver. 10.5 (Molecular Devices, CA, USA) and Excel (Microsoft, Washington, USA) software. All data were presented as mean values ± SE, where each duration time was taken using the natural logarithm. Channel current measurements were conducted at room temperature (22 ± 2 °C). All operations were conducted from three to five times ($3 < N < 5$) with different nanopores, and all DNA transitions were observed from 400 to 1700 times ($400 < n < 1700$) in each nanopore. The definitions for "dwell time of open level" and "event frequency", appearing in Figure 3, and "dwell time" and "ratio of dwell time", appearing in Figure 4, are as follows:

Dwell time of open level: time from the open pore of αHL to the blocking by an hpDNA
Event frequency: number of transition events per second
Dwell time: mean dwell time of each state
Ratio of dwell time: total dwell time of each state/time of all states

RESULTS AND DISCUSSION

Nanopore Conductance in Glycerol and PEG Solution. Prior to performing the hpDNA experiment, the conductance of αHL nanopores in glycerol and PEG600 solutions was initially

https://dx.doi.org/10.1021/acs.jpcb.9b11096
J. Phys. Chem. B 2020, 124, 2410−2416

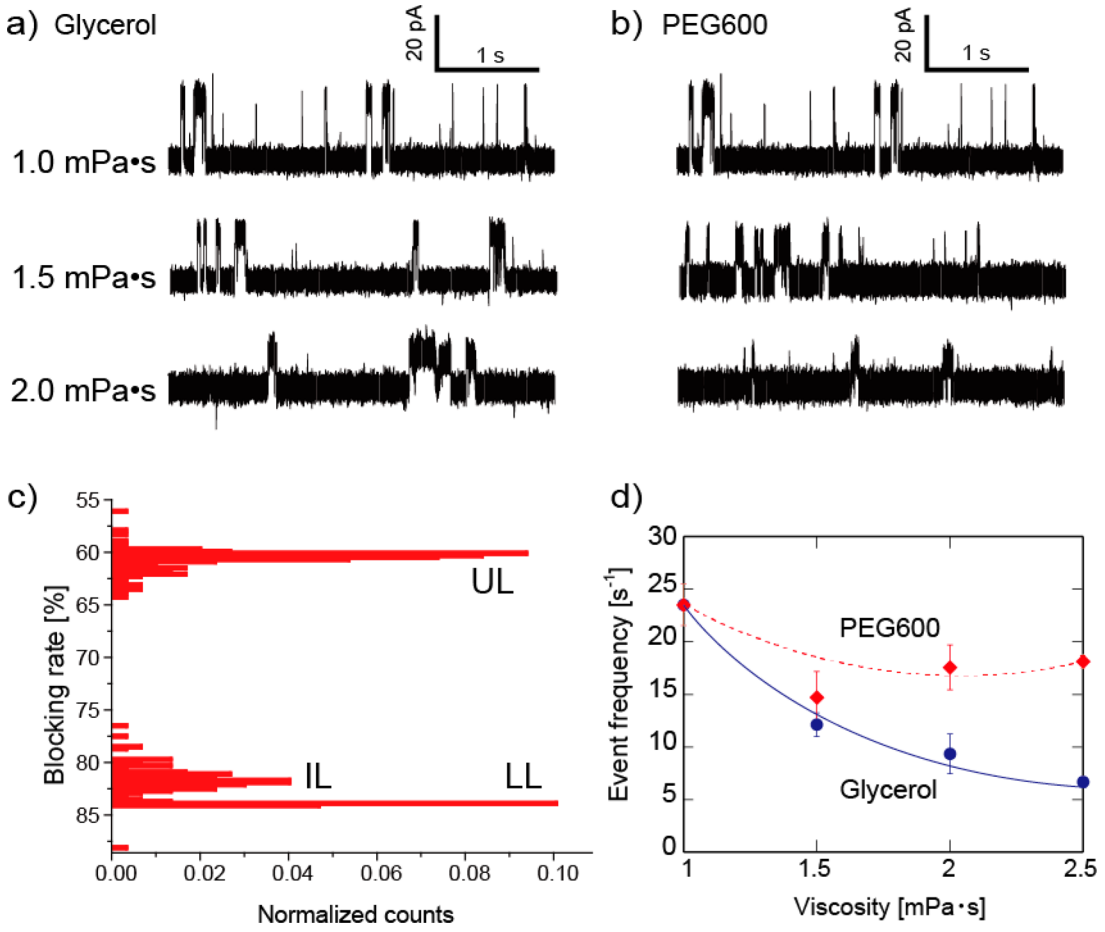

Figure 3. (a, b) Typical transition signal of (a) glycerol and (b) PEG600 in each solution (V_{app} = +120 mV). (c) Typical histogram of blocking currents at each transition level in glycerol solution (2.0 mPa s). (d) Event frequency of hpDNA transition in each solution.

examined in order to compare their behavior in bulk solution. Parts a and b of Figure 2 show the open channel amplitudes of the αHL pore in glycerol and PEG600 solutions. The open currents decrease with increasing viscosity in both solutions. The current and voltage curves in each solution are also shown in Figure S1. The conductivity in the bulk and in the nanopore can be theoretically defined as follows[41]

Bulk:

$$\sigma_{bulk} = \sum_i (n_i z_i \mu_i)$$

Nanopore:.

$$G_{pore} = F\left(\frac{V_{pore}}{d_{pore}^{\ 2}}\right)\sum_i (z_i c_i \mu_i)$$

$$\mu = \frac{z_i e}{6\pi r\eta}$$

where σ_{bulk} is the conductivity (S cm^{-1}) in bulk solution. G_{pore} is the conductance (S) of the nanopore. n, z, c, μ, r, and η are the carrier density, the charge of the carrier, the concentration, the mobility, the Stokes radius, and the viscosity, respectively, of the ith mobile species. F is Faraday's constant, and V_{pore} and d_{pore} are the volume and length of the nanopore. According to these equations, the conductance has an inverse proportional relationship with the viscosity. Figure 2c depicts the viscosity dependence of the conductance with glycerol and PEG600 and the predicted value from the bulk solution. The predicted value provides the bulk conductance of both the glycerol and PEG600 solutions theoretically. The conductance in both solutions shows an inverse proportion with the viscosity as well as the predicted value. Interestingly, although the pore conductance in the glycerol solution was lower than that of the predicted value, the conductance of the PEG600 solution was higher than the predicted value even at the same viscosity. The mobility of ions or small molecules should decrease in the confined nanospace because the surface area of the wall in the nanospace is large, and the experimental results support the low mobility of water molecules in the nanospace of the glycerol solution.[42] In contrast to the PEG600 system, there are three possible reasons for the higher conductance: (1) the concentration (c) of ions in the nanospace is different in bulk solution, (2) the mobility of ions (μ) in the nanospace is different in bulk solution, or (3) both 1 and 2. Next, we attempt to reveal the mechanism for the above-mentioned phenomenon using hpDNA in terms of these three hypotheses.

Entry Kinetics of hpDNA into the αHL Pore. Figure 2d presents the time from "αHL pore opening" to "hpDNA entrance into the pore vestibule", called the "dwell time of the open level", of each solution. In the case of the glycerol solution, the dwell time was virtually constant in this viscosity range. In contrast to the PEG600 solution, the entrance time shortened with increasing viscosity. The hpDNA rapidly entered the nanopores even in the higher viscosity solution. This

https://dx.doi.org/10.1021/acs.jpcb.9b11096
J. Phys. Chem. B 2020, 124, 2410−2416

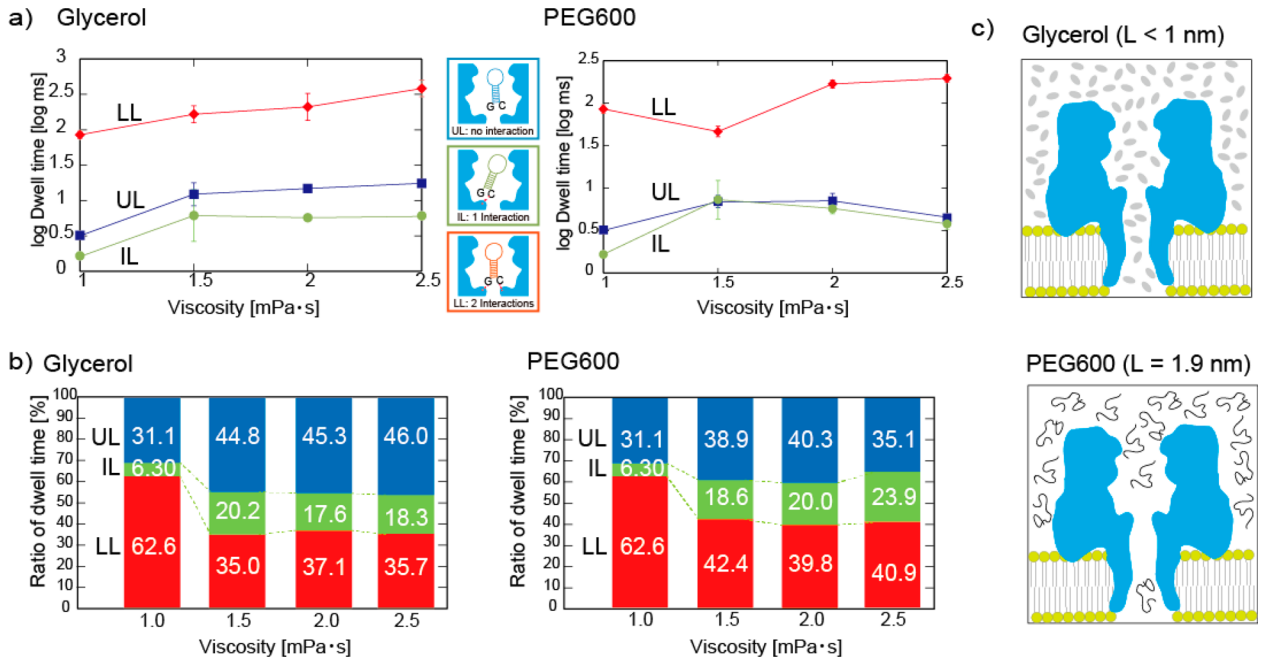

Figure 4. Dwell time of each state (UL, IL, and LL, V_{app} = +120 mV). (a) Average time of all events in each state. Dwell time = mean dwell time of each state. (b) Ratio of each dwell time in total blockings. Sum of the entire time of each state. For example, ratio of LL state = (time of total LL state)/(time of all states). (c) Schematic illustration of the glycerol and PEG600 systems. The *L* value indicates the approximate size of each molecule.

phenomenon would be explained by a depletion force. Possibly due to the low concentration of PEG600 in the inner space of the pore, the hpDNA existing near the pore entrance should be pressed by the circumambient PEG molecules into the nanopore, resulting in its rapid entry.

A low PEG concentration state in the pore can well explain the higher conductance of the PEG system because the ions (K^+ and Cl^-) in the pore have high mobilities and/or high concentrations in the pore. From another viewpoint, the difference of molecular phase between the inside and outside of the pore can be considered as the separation mechanism in the PEG600 system. Phase separation in confined spaces, especially in living cells, has been reported in cell biology.[43] The confined nanospace can induce phase separation. The measurement results for the PEG600 solution indicate that there may be different phases present: a high polymer condensed phase in the outside bulk and a low polymer condensed phase in the inside pore. Considering these results, we concluded that our hypothesis of "(3) both 1 and 2" provides a reasonable explanation for the unusual conductance phenomenon of the nanospace in the PEG600 aqueous environment.

Modulation of hpDNA in the Nanopore Reflects the Different Nanoenvironments between the Glycerol and PEG600 Solutions. It has been previously reported that an hpDNA with nine base pairs having a GC terminus has three stable current states: upper (**UL**), intermediate (**IL**), and lower levels (**LL**).[35] These states reflect three different interactions between the terminus bases and the pore wall in the αHL vestibule (see Figure 1a). In the case of **UL**, the terminus of hpDNA, GC in this case, does not interact with the inside wall of the pore, orienting along with the central pore region, resulting in a large current flowing. **IL** is observed when one of the ends of hpDNA interacts with the restriction region of αHL and shows medium current blocking. **LL**, the deepest current state, occurs when both termini interact with the pore vestibule and shows the highest current blocking state.[36]

The hpDNA with GC terminus also showed clear transition signals in both glycerol and PEG600 solutions after injection into the nanopore; the typical current and time traces are presented in Figure 3a and b. The transition amplitudes became smaller with increasing viscosity. The histogram of the blocking current also indicates the three states, **UL**, **IL**, and **LL**, even in the viscous solutions of glycerol and PEG600; the typical result is shown in Figure 3c, and all histograms are shown in Figure S2.

Next, we analyze the viscosity dependence of the transition-event frequency of [**IL**] ⇆ [**UL**] ⇆ [**LL**] (Figure 3d). This transition reflects the molecular motility in the confined nanospace, as also reported previously.[44] In the case of the glycerol solution, the event frequency became slow, suggesting that each state became stable with increasing viscosity (increasing the concentration of glycerol). The energy barrier of the transition reaction rose in the more viscous solution. On the other hand, in the PEG600 solution, the frequency decreased from the 1 to 1.5 mPa s solution. However, the frequency was subsequently virtually constant or slightly increased. This result indicated that hpDNA moved independently of the viscosity changing with the PEG600 solution in the nanospace.

We next focus on the transition events of [**IL**] ⇆ [**UL**] ⇆ [**LL**] and estimate the inner environment of the nanopore with two different viscous solutions. It has been proposed that these three states correspond to the difference in the number of the hydrogen bonds between the terminus hpDNA and the restricted region of the αHL pore: **UL**, **IL**, and **LL** have zero, one, and two hydrogen bonds, respectively.[35] Figure 4a shows the dwell time of each state in both the glycerol and PEG600 solutions. In the glycerol solution, the dwell time of all three states became longer with increasing viscosity. Probably due to the effect of the increasing viscosity, each state should become stable; in other words, the energy barrier of the transition may become high, inhibiting the state transition reaction. These results correspond to the results from the transition analysis, as mentioned above. In contrast to the glycerol system, the dwell

https://dx.doi.org/10.1021/acs.jpcb.9b11096
J. Phys. Chem. B 2020, 124, 2410−2416

time of the **LL** and **UL** states becomes slightly shorter with increasing PEG600 concentration. This result implies the occurrence of destabilization of each state by the PEG600 addition. However, the change is too small to make a clear description. To analyze the details on the dwell time, the ratio of each dwell time in the total signal appearance was analyzed, as shown in Figure 4b. The reduction of **LL** in the glycerol system is larger than that in the PEG600 system, and the **UL** slightly increases in glycerol compared with the PEG600 system. This tendency may indicate that a glycerol molecule inhibits the interaction between hpDNA and the αHL wall, probably because of its hydrogen bonding ability. In contrast, the PEG has weak hydrogen bonding ability and it can make each hpDNA state stable.

The two viscous systems in the confined nanospace are differentiated schematically in Figure 4c. Glycerol (as a small-sized molecule) exists in the nanospace as in the bulk solution, and each molecule interacts via hydrogen bonding in the narrow area, inhibiting the mobility of ions and hpDNA. On the other hand, in the PEG600 system (as a polymer), the number of molecules in the nanospace is less than that in the bulk solution, and each polymer interacts with an entanglement of the polymer chains, relatively not inhibiting the mobility of ions and hpDNA.

CONCLUSIONS

In summary, we observed and characterized the single confined nanospace of an αHL nanopore with hpDNA. Using this system, we measured the channel conductance and molecular motion of hpDNA in the αHL nanopore and compared the macro- and nanospace using two different viscous molecules: glycerol and PEG600. Two important findings were made: (1) The channel conductance in the PEG system was higher than that in the glycerol system, suggesting that the concentration of PEG in the nanospace is lower than that in the macrospace. This result implies high ion mobility or concentration in the nanospace. (2) In the nanospace, glycerol and PEG600 have different effects on the molecular motion of hpDNA even when their viscosities are the same in the bulk solution. These differences are due to differences in the mechanism of viscosity between glycerol and PEG600: the viscosity induced by glycerol is due to hydrogen-bonding-based interactions, while the viscosity induced by PEG600 is due to entanglement of the polymer chains. These differences can be observed clearly by using the biological nanopore and hpDNA.

As the next step, we have integrated this system with a gold nanoneedle to construct a spatially resolved nanopore probe, as we recently proposed.[45] The hpDNA was able to be inserted into the αHL pore, as indicated by the blocking current (Figure S3). This system can be further improved for applications such as living cell imaging.

ASSOCIATED CONTENT

Supporting Information

The Supporting Information is available free of charge at https://pubs.acs.org/doi/10.1021/acs.jpcb.9b11096.

The device fabrications and detailed experimental data are available (PDF)

AUTHOR INFORMATION

Corresponding Author

Ryuji Kawano − *Department of Biotechnology and Life Science, Tokyo University of Agriculture and Technology, Koganei-shi, Tokyo 184-8588, Japan;* orcid.org/0000-0001-6523-0649; Email: rjkawano@cc.tuat.ac.jp

Authors

Masaki Matsushita − *Department of Biotechnology and Life Science, Tokyo University of Agriculture and Technology, Koganei-shi, Tokyo 184-8588, Japan*

Kan Shoji − *Department of Biotechnology and Life Science, Tokyo University of Agriculture and Technology, Koganei-shi, Tokyo 184-8588, Japan; Department of Chemistry, University of Cincinnati, Cincinnati, Ohio 45221, United States;* orcid.org/0000-0002-7198-9683

Natsumi Takai − *Department of Biotechnology and Life Science, Tokyo University of Agriculture and Technology, Koganei-shi, Tokyo 184-8588, Japan*

Complete contact information is available at: https://pubs.acs.org/10.1021/acs.jpcb.9b11096

Author Contributions

M.M. and R.K. conceived the original idea. M.M., K.S., and N.T. conducted the experiments and analyzed the data. R.K. and M.M. wrote the paper. All authors have given approval to the final version of the manuscript.

Notes

The authors declare no competing financial interest.

ACKNOWLEDGMENTS

This work was partly supported by KAKENHI (Grant Nos. 17K19138, 19H00901) from MEXT, Japan.

REFERENCES

(1) Crupi, V.; Dianoux, A. J.; Majolino, D.; Migliardo, P.; Venuti, V. Dynamical response of liquid water in confined geometry by laser and neutron spectroscopies. *Phys. Chem. Chem. Phys.* **2002**, *4* (12), 2768−2773.

(2) Christenson, H. K. Confinement effects on freezing and melting. *J. Phys.: Condens. Matter* **2001**, *13* (11), R95−R133.

(3) Dore, J. Structural studies of water in confined geometry by neutron diffraction. *Chem. Phys.* **2000**, *258* (2−3), 327−347.

(4) Baker, J. M.; Dore, J. C.; Behrens, P. Nucleation of ice in confined geometry. *J. Phys. Chem. B* **1997**, *101* (32), 6226−6229.

(5) Steytler, D. C.; Dore, J. C. Neutron-diffraction studies of water in porous silica 0.2. Temperature-variation in the super-cooled regime. *Mol. Phys.* **1985**, *56* (5), 1001−1015.

(6) Koga, K.; Gao, G. T.; Tanaka, H.; Zeng, X. C. Formation of ordered ice nanotubes inside carbon nanotubes. *Nature* **2001**, *412* (6849), 802−805.

(7) Bruni, F.; Ricci, M. A.; Soper, A. K. Water confined in Vycor glass. I. A neutron diffraction study. *J. Chem. Phys.* **1998**, *109* (4), 1478−1485.

(8) Agrawal, K. V.; Shimizu, S.; Drahushuk, L. W.; Kilcoyne, D.; Strano, M. S. Observation of extreme phase transition temperatures of water confined inside isolated carbon nanotubes. *Nat. Nanotechnol.* **2017**, *12* (3), 267−273.

(9) Perez, M. Gibbs-Thomson effects in phase transformations. *Scr. Mater.* **2005**, *52* (8), 709−712.

(10) Tsukahara, T.; Hibara, A.; Ikeda, Y.; Kitamori, T. NMR study of water molecules confined in extended nanospaces. *Angew. Chem., Int. Ed.* **2007**, *46* (7), 1180−1183.

(11) Hibara, A.; Saito, T.; Kim, H. B.; Tokeshi, M.; Ooi, T.; Nakao, M.; Kitamori, T. Nanochannels on a fused-silica microchip and liquid properties investigation by time-resolved fluorescence measurements. *Anal. Chem.* **2002**, *74* (24), 6170−6176.

(12) Grunberg, B.; Emmler, T.; Gedat, E.; Shenderovich, I.; Findenegg, G. H.; Limbach, H. H.; Buntkowsky, G. Hydrogen bonding of water confined in mesoporous silica MCM-41 and SBA-15 studied by H-1 solid-state NMR. *Chem. - Eur. J.* **2004**, *10* (22), 5689−5696.

(13) Morineau, D.; Xia, Y. D.; Alba-Simionesco, C. Finite-size and surface effects on the glass transition of liquid toluene confined in cylindrical mesopores. *J. Chem. Phys.* **2002**, *117* (19), 8966−8972.
(14) Molz, E.; Wong, A. P. Y.; Chan, M. H. W.; Beamish, J. R. Freezing and melting of fluids in porous glasses. *Phys. Rev. B: Condens. Matter Mater. Phys.* **1993**, *48* (9), 5741−5750.
(15) Rovere, M.; Ricci, M. A.; Vellati, D.; Bruni, F. A molecular dynamics simulation of water confined in a cylindrical SiO2 pore. *J. Chem. Phys.* **1998**, *108* (23), 9859−9867.
(16) Liu, Y. C.; Wang, Q.; Lu, L. H. Water confined in nanopores: its molecular distribution and diffusion at lower density. *Chem. Phys. Lett.* **2003**, *381* (1−2), 210−215.
(17) Hummer, G.; Rasaiah, J. C.; Noworyta, J. P. Water conduction through the hydrophobic channel of a carbon nanotube. *Nature* **2001**, *414* (6860), 188−190.
(18) Song, L.; Hobaugh, M. R.; Shustak, C.; Cheley, S.; Bayley, H.; Gouaux, J. E. Structure of staphylococcal alpha-hemolysin, a heptameric transmembrane pore. *Science* **1996**, *274* (5294), 1859−1865.
(19) Deamer, D. W.; Branton, D. Characterization of nucleic acids by nanopore analysis. *Acc. Chem. Res.* **2002**, *35* (10), 817−825.
(20) Branton, D.; Deamer, D. W.; Marziali, A.; Bayley, H.; Benner, S. A.; Butler, T.; Di Ventra, M.; Garaj, S.; Hibbs, A.; Huang, X.; et al. The potential and challenges of nanopore sequencing. *Nat. Biotechnol.* **2008**, *26* (10), 1146−1153.
(21) Howorka, S.; Siwy, Z. Nanopore analytics: sensing of single molecules. *Chem. Soc. Rev.* **2009**, *38* (8), 2360−84.
(22) Wanunu, M. Nanopores: A journey towards DNA sequencing. *Phys. Life Rev.* **2012**, *9* (2), 125−158.
(23) Kasianowicz, J. J.; Brandin, E.; Branton, D.; Deamer, D. W. Characterization of individual polynucleotide molecules using a membrane channel. *Proc. Natl. Acad. Sci. U. S. A.* **1996**, *93* (24), 13770−13773.
(24) Gu, L. Q.; Braha, O.; Conlan, S.; Cheley, S.; Bayley, H. Stochastic sensing of organic analytes by a pore-forming protein containing a molecular adapter. *Nature* **1999**, *398* (6729), 686−690.
(25) Gu, L. Q.; Shim, J. W. Single molecule sensing by nanopores and nanopore devices. *Analyst* **2010**, *135* (3), 441−451.
(26) Reiner, J. E.; Balijepalli, A.; Robertson, J. W.; Campbell, J.; Suehle, J.; Kasianowicz, J. J. Disease detection and management via single nanopore-based sensors. *Chem. Rev.* **2012**, *112* (12), 6431−6451.
(27) Osaki, T.; Takeuchi, S. Artificial Cell Membrane Systems for Biosensing Applications. *Anal. Chem.* **2017**, *89* (1), 216−231.
(28) Kawano, R. Nanopore Decoding of Oligonucleotides in DNA Computing. *Biotechnol. J.* **2018**, *13* (12), 1800091.
(29) Cao, C.; Long, Y. T. Biological Nanopores: Confined Spaces for Electrochemical Single-Molecule Analysis. *Acc. Chem. Res.* **2018**, *51* (2), 331−341.
(30) An, N.; Fleming, A. M.; White, H. S.; Burrows, C. J. Nanopore detection of 8-oxoguanine in the human telomere repeat sequence. *ACS Nano* **2015**, *9* (4), 4296−4307.
(31) Johnson, R. P.; Fleming, A. M.; Perera, R. T.; Burrows, C. J.; White, H. S. Dynamics of a DNA Mismatch Site Held in Confinement Discriminate Epigenetic Modifications of Cytosine. *J. Am. Chem. Soc.* **2017**, *139* (7), 2750−2756.
(32) Jeong, K. B.; Luo, K.; Lee, H.; Lim, M. C.; Yu, J.; Choi, S. J.; Kim, K. B.; Jeon, T. J.; Kim, Y. R. Alpha-Hederin Nanopore for Single Nucleotide Discrimination. *ACS Nano* **2019**, *13* (2), 1719−1727.
(33) Bonome, E. L.; Cecconi, F.; Chinappi, M. Translocation intermediates of ubiquitin through an α-hemolysin nanopore: implications for detection of post-translational modifications. *Nanoscale* **2019**, *11* (20), 9920−9930.
(34) Vercoutere, W.; Winters-Hilt, S.; Olsen, H.; Deamer, D.; Haussler, D.; Akeson, M. Rapid discrimination among individual DNA hairpin molecules at single-nucleotide resolution using an ion channel. *Nat. Biotechnol.* **2001**, *19* (3), 248−252.
(35) Vercoutere, W. A.; Winters-Hilt, S.; DeGuzman, V. S.; Deamer, D.; Ridino, S. E.; Rodgers, J. T.; Olsen, H. E.; Marziali, A.; Akeson, M. Discrimination among individual Watson-Crick base pairs at the termini of single DNA hairpin molecules. *Nucleic Acids Res.* **2003**, *31* (4), 1311−1318.
(36) DeGuzman, V. S.; Lee, C. C.; Deamer, D. W.; Vercoutere, W. A. Sequence-dependent gating of an ion channel by DNA hairpin molecules. *Nucleic Acids Res.* **2006**, *34* (22), 6425−6437.
(37) Kawano, R.; Tsuji, Y.; Sato, K.; Osaki, T.; Kamiya, K.; Hirano, M.; Ide, T.; Miki, N.; Takeuchi, S. Automated Parallel Recordings of Topologically Identified Single Ion Channels. *Sci. Rep.* **2013**, *3*, 1995.
(38) Ohara, M.; Sekiya, Y.; Kawano, R. Hairpin DNA Unzipping Analysis Using a Biological Nanopore Array. *Electrochemistry* **2016**, *84* (5), 338−341.
(39) Segur, J. B.; Oberstar, H. E. Viscosity of glycerol and its aqueous solutions. *Ind. Eng. Chem.* **1951**, *43* (9), 2117−2120.
(40) Kirincic, S.; Klofutar, C. Viscosity of aqueous solutions of poly(ethylene glycol)s at 298.15 K. *Fluid Phase Equilib.* **1999**, *155* (2), 311−325.
(41) Kawano, R.; Schibel, A. E. P.; Cauley, C.; White, H. S. Controlling the Translocation of Single-Stranded DNA through alpha-Hemolysin Ion Channels Using Viscosity. *Langmuir* **2009**, *25* (2), 1233−1237.
(42) Li, L. X.; Kazoe, Y.; Mawatari, K.; Sugii, Y.; Kitamori, T. Viscosity and Wetting Property of Water Confined in Extended Nanospace Simultaneously Measured from Highly-Pressurized Meniscus Motion. *J. Phys. Chem. Lett.* **2012**, *3* (17), 2447−2452.
(43) Shin, Y.; Brangwynne, C. P. Liquid phase condensation in cell physiology and disease. *Science* **2017**, *357* (6357), eaaf4382.
(44) Asandei, A.; Schiopu, I.; Chinappi, M.; Seo, C. H.; Park, Y.; Luchian, T. Electroosmotic Trap Against the Electrophoretic Force Near a Protein Nanopore Reveals Peptide Dynamics During Capture and Translocation. *ACS Appl. Mater. Interfaces* **2016**, *8* (20), 13166−13179.
(45) Shoji, K.; Kawano, R.; White, R. J. Spatially Resolved Chemical Detection with a Nanoneedle-Probe-Supported Biological Nanopore. *ACS Nano* **2019**, *13* (2), 2606−2614.

https://dx.doi.org/10.1021/acs.jpcb.9b11096
J. Phys. Chem. B 2020, 124, 2410−2416